Drug Design, Development and Therapy

Dovepress

open access to scientific and medical research

Open Access Full Text Article

ORIGINAL RESEARCH

Parabacteroides distasonis-Derived Outer Membrane Vesicles Enhance Antitumor Immunity Against Colon Tumors by Modulating CXCL10 and $CD8^+$ T Cells

Rongyao Liang[1,*], Pei Li[1,2,*], Na Yang[1], Xiaoyi Xiao[1], Jing Gong[1], Xingyuan Zhang[1], Yunuan Bai[1], Yanlong Chen[1], Zhiyong Xie[3], Qiongfeng Liao[1]

[1]School of Pharmaceutical Sciences, Guangzhou University of Chinese Medicine, Guangzhou, Guangdong Province, People's Republic of China; [2]Science and Technology Innovation Center, Guangzhou University of Chinese Medicine, Guangzhou, Guangdong Province, People's Republic of China; [3]School of Pharmaceutical Sciences (Shenzhen), Sun Yat-sen University, Shenzhen, Guangdong Province, People's Republic of China

*These authors contributed equally to this work

Correspondence: Qiongfeng Liao, School of Pharmaceutical Sciences, Guangzhou University of Chinese Medicine, Guangzhou, 510006, People's Republic of China, Tel +86 2039358081, Email zyfxliao@gzucm.edu.cn; Zhiyong Xie, School of Pharmaceutical Sciences (Shenzhen), Sun Yat-sen University, Guangzhou, 510006, People's Republic of China, Tel +86 075523260207, Email xiezhy@mail.sysu.edu.cn

Purpose: Given the potent immunostimulatory effects of bacterial outer membrane vesicles (OMVs) and the significant anti-colon tumor properties of *Parabacteroides distasonis* (*Pd*), this study aimed to elucidate the role and potential mechanisms of *Pd*-derived OMVs (*Pd*-OMVs) against colon cancer.

Methods: This study isolated and purified *Pd*-OMVs from *Pd* cultures and assessed their characteristics. The effects of *Pd*-OMVs on CT26 cell uptake, proliferation, and invasion were investigated in vitro. In vivo, a CT26 colon tumor model was used to investigate the anti-colon tumor effects and underlying mechanisms of *Pd*-OMVs. Finally, we evaluated the biosafety of *Pd*-OMVs.

Results: Purified *Pd*-OMVs had a uniform cup-shaped structure with an average size of 165.5 nm and a zeta potential of approximately −9.56 mV, and their proteins were associated with pathways related to immunity and apoptosis. In vitro experiments demonstrated that CT26 cells internalized the *Pd*-OMVs, resulting in a significant decrease in their proliferation and invasion abilities. Further in vivo studies confirmed the accumulation of *Pd*-OMVs in tumor tissues, which significantly inhibited the growth of colon tumors. Mechanistically, *Pd*-OMVs increased the expression of CXCL10, promoting infiltration of $CD8^+$ T cells into tumor tissues and expression of pro-inflammatory factors TNF-α, IL-1β, and IL-6. Notably, *Pd*-OMVs demonstrated a high level of biosafety.

Conclusion: This paper elucidates that *Pd*-OMVs can exert significant anti-colon tumor effects by upregulating the expression of the chemokine CXCL10, thereby increasing the infiltration of $CD8^+$ T cells into tumors and enhancing antitumor immune responses. This suggests that *Pd*-OMVs may be developed as a novel nanoscale potent immunostimulant with great potential for application in tumor immunotherapy. As well as developed as a novel nano-delivery carrier for combination with other antitumor drugs.

Keywords: *Parabacteroides distasonis*, outer membrane vesicles, colon tumor, CXCL10, $CD8^+$ T cells

Introduction

Colon cancer ranks as the third leading cause of cancer-related deaths, being one of the most prevalent gastrointestinal malignancies. There is growing evidence that the incidence of colon cancer is rapidly increasing among young individuals.[1,2] The increased risk of colon cancer is strongly linked to unhealthy lifestyle factors like smoking, high sugar diets, excessive alcohol consumption and inadequate physical activity.[3] The treatment modalities for colon cancer include surgery, radiation therapy, chemotherapy, and immunotherapy. Depending on the location of the cancer, number of metastases and tumor progression, colon cancer patients may receive an individualized treatment strategy. For

Received: 30 December 2023
Accepted: 16 May 2024
Published: 28 May 2024

Graphical Abstract

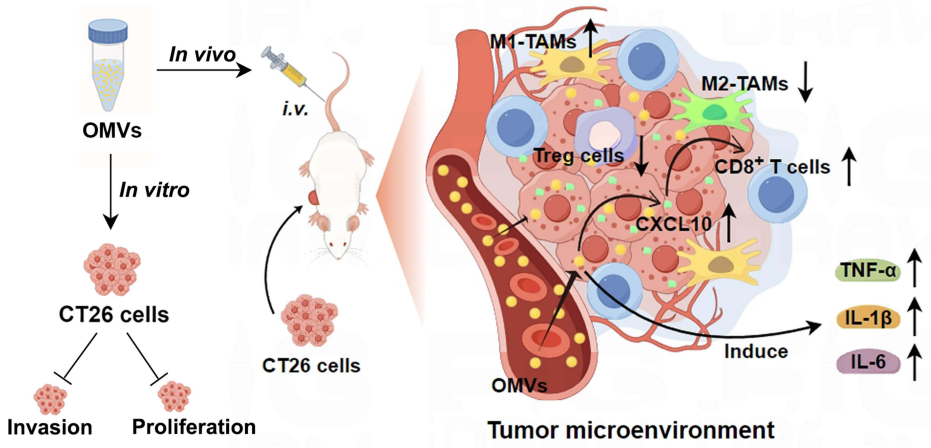

chemotherapy, approved drugs are commonly used, including bevacizumab, irinotecan hydrochloride and capecitabine.[4] However, these drugs tend to cause serious adverse effects in the digestive tract and nervous system during clinical treatment. Additionally, drug resistance and organ toxicity of chemotherapeutic drugs are also the key problems faced by chemotherapy.[5] In recent years, tumor immunotherapy has emerged as a promising frontier therapy in the field of fighting cancer, providing a new strategy to utilize the immune system for tumor eradication. Although immunotherapy has shown impressive efficacy and fewer adverse effects in some patients, studies have shown that existing immunotherapeutic agents also suffer from low response rates and overall success rates.[6] Therefore, the development of novel tumor immunotherapy drugs highlights the important of practical significance.

Parabacteroides distasonis (*Pd*), a gram-negative bacterium and a vital component of the human intestinal microbiota, emerges as a second-generation probiotic with diverse probiotic properties.[7,8] Studies have found that *Pd* could reduce obesity, ameliorate colitis, type 2 diabetes, inflammatory arthritis and liver fibrosis.[9–13] Notably, *Pd* demonstrated effective inhibitory effects on colon cancer, as evidenced by reducing the TLR4 activation and preventing the formation of colon tumor.[14,15] However, despite the remarkable antitumor properties of *Pd*, bacteria use in tumor therapy has raised concerns about toxic side effects, necessitating the exploration of safe and reliable alternatives.[16]

Outer membrane vesicles (OMVs), extracellular vesicles originating from the outer membrane of gram-negative bacteria, present a potential solution. Characterized by a cup-shaped structure and an average diameter ranging from 20 to 500 nm, OMVs offer distinct safety advantages over live or attenuated bacteria.[17] As non-replicating bacterial entities, OMVs mitigate safety concerns associated with systemic infections and adverse events linked to probiotic administration.[18] Furthermore, OMVs have the advantages of being economical, mass-producible, and biologically safe. Significantly, OMVs have exhibited a range of beneficial effects, including antitumor and immunostimulatory properties, opening avenues for their application in tumor immunotherapy.[19,20] Vaccines made from Neisseria meningitidis-derived OMVs were approved many years ago for preventing human meningococcal disease.[21] Several recent studies have shown the great potential of various bacterial-derived OMVs in tumor therapy, drug delivery, and vaccine development.[18] *Escherichia coli*-OMVs have been shown to upregulate the expressions of CXCL10 and interferon-γ, thereby effectively enhancing antitumor immunity and completely eradicating formed tumors.[22,23] OMVs derived from *Salmonella typhimurium* have been observed to strongly stimulated antitumor immune response and ablate tumor by reversing the immunosuppressed tumor microenvironment.[24] *Akkermansia muciniphila*-derived OMVs efficiently induced the antitumor immune response by promoting dendritic cells maturation and activating cytotoxic T cells responses, thereby inhibiting tumor growth.[25] These findings underscore the

optimistic prospect of employing bacteria-derived vesicles in immunotherapy, making them attractive candidates for biomedical applications, including tumor immunotherapy.[26] Additionally, OMVs can carry various components from their parent cells, including lipopolysaccharides, RNAs, outer membrane proteins, and lipids, thus facilitating intercellular communication between bacteria and hosts.[27–29] Given that previous studies have revealed the anti-colon tumor properties of *Pd*, further investigation into the efficacy of *Pd*-derived OMVs (*Pd*-OMVs) in combatting colon tumor is warranted.

To achieve this, our research encompasses both in vitro and in vivo studies. Initially, *Pd*-OMVs were isolated from *Pd* cultures and characterized. The uptake capacity of CT26 cells for *Pd*-OMVs and the anti-colon tumor activities of *Pd*-OMVs were evaluated in vitro. The antitumor effects of *Pd*-OMVs administered intratumorally and intravenously was explored using the CT26 tumor model in vivo. Transcriptomics was employed to reveal the potential mechanisms of *Pd*-OMVs. Finally, the biosafety of *Pd*-OMVs was evaluated. This pioneering study explored the potential inhibitory effects of *Pd*-OMVs on colon tumors for the first time, highlighting the great promise and clinical translational value of *Pd*-OMVs as a novel immunotherapeutic agent. However, there are still challenges for the realization of their clinical translation, including the requirement for more comprehensive and systematic pharmacological and toxicological studies, as well as scientific and standardized clinical trials. Therefore, this study aims to build a solid experimental foundation and scientific basis for further research and development of *Pd*-OMVs.

Materials and Methods

Chemicals and Reagents

Brain Heart Infusion (BHI) broth was obtained from BD (New Jersey, USA). 3.3'-dioctadecyloxacarbocyanine perchlorate (DIO), 1.1'-dioctadecyl-3,3,3',3'-tetramethylindocarbocyanine perchlorate (DIL) and 2-(4-Amidinophenyl)-6-indolecarbamidine dihydrochloride (DAPI) were obtained from Beyotime (Shanghai, China). DMEM and RPMI 1640 medium were obtained from Gibco (MA, USA). The CCK8 assay kit and 5-Fluorouracil (5-Fu) were purchased from APExBIO (TX, USA). Enzyme-linked immunosorbent assay (ELISA) kits for TNF-α, IL-1β and IL-6 were obtained from ABclonal Biology Co., Ltd. (Wuhan, China). ELISA kit for C-X-C motif chemokine ligand 10 (CXCL10) was obtained from Multisciences Biotech Co., Ltd. (Hangzhou, China). Alkaline phosphatase (ALP), alanine aminotransferase (ALT), aspartate aminotransferase (AST) and urea nitrogen (BUN) assay kits, Matrigel Basement Membrane Matrix, Collagenase II, Collagenase IV and DNase I were obtained from Solarbio (Beijing, China). Creatinine (CRE) assay kit was obtained from Nanjing Jiancheng Bioengineering institute (Nanjing, China). Zombie Aqua™ Fixable Viability Kit, APC/cy7 CD3, FITC CD4, APC CD25, PE/cy7 CD45, Alexa Fluor® 700 CD11b, BV421 CD86, APC CD206, APC CD8, PE Granzyme B (GrB) and FITC F4/80 anti-mouse antibodies were obtained from BioLegend (San Diego, CA, USA). PE Foxp3 and anti-CXCL10 antibody (clone 134,013) were obtained from Thermo Fisher Scientific (Waltham, MA, USA). HiFiScript gDNA Removal RT MasterMix and MagicSYBR Mixture for qPCR were obtained from CWBIO (Jiangsu, China). Ki67 and CD8 antibodies for IHC were obtained from Servicebio (Wuhan, China). CXCL10 antibody for IHC was obtained from Proteintech (Wuhan, China).

Bacterial Culture and *Pd*-OMVs Purification

A previously reported method was used to obtain *Pd*-OMVs from *Pd* cultures.[20,30] In brief, *Parabacteroides distasonis*, obtained from ATCC (ATCC 8503), was subcultured in BHI broth with 150 × *g* shaking at 37°C for 48 h under anaerobic conditions. The *Pd* cultures were then transferred to centrifuge tubes and centrifuged twice at 10,000 × *g* for 20 min at 4°C. The supernatant was then filtered through a 0.45 μm pore size filter and the filtrate was collected to remove residual bacteria and cellular debris. The cell-free filtrate was then ultracentrifuged at 150,000 × *g* for 2 h at 4°C. The supernatant was discarded to obtain the *Pd*-OMVs precipitates. For purification, the *Pd*-OMVs precipitates were resuspended in sterile phosphate-buffered saline (PBS), transferred to ultrafiltration centrifuge tubes (30 kDa), and then centrifuged at 8000 × *g* for 30 min at 4°C to collect the *Pd*-OMVs suspension. Finally, the purified *Pd*-OMVs suspension was filtered through a 0.22 μm pore size filter to remove impurities and ensure sterility. The sterile *Pd*-OMVs were then dispensed

and stored at –80°C until further use. The protein concentration in the samples was determined using the bisquinaldic acid assay.

Pd-OMVs Characterization

To conduct transmission electron microscopy (TEM) analysis, *Pd*-OMVs were applied to a 150-mesh copper grid and subsequently stained with a solution containing 2% uranyl acetate. Images were taken at an accelerating voltage of 100 kV. Dynamic light scattering (DLS) analysis, for determining the size and zeta potential of the *Pd*-OMVs, was performed using a Zetasizer Nano ZS instrument. The reported results represent the average of three distinct measurements.

Proteomics

The *Pd*-OMVs were extracted and characterized for proteomics analysis. Detailed proteomics analysis methods can be found in Supplementary Methods. The mass spectrometry proteomics data have been deposited to the ProteomeXchange Consortium (https://proteomecentral.proteomexchange.org) via the iProX partner repository with the dataset identifier PXD051464.

Cells Culture

The murine colon cancer cell line CT26 was cultured in 1640 medium supplemented with 10% FBS and 1% penicillin/streptomycin at 5% CO_2 and 37°C. HCT116 and SW480, two human colon cancer cell lines, were cultivated in DMEM medium supplemented with 10% FBS and 1% penicillin/streptomycin under identical culture conditions of 5% CO_2 and 37°C. All cell lines utilized in this study were procured from the Cell Bank of the Chinese Academy of Sciences.

In vitro Cellular Uptake Profiles of OMVs

DIO solution (1×10^{-5} mol/L) was added to the OMVs suspension (protein concentration: 1 mg/mL, 1 mL). Subsequently, the solution was incubated for 30 min at 37°C. The free DIO was removed using a 30 kDa ultracentrifuge filter, and the purified DIO-labeled OMVs were obtained. After inoculating in 24-well plates, CT26 cells were grown for a whole night. Medium containing 0 or 400 μg/mL DIO-labeled OMVs was substituted for the whole medium. The cells were co-cultured for 5 h, and then extra OMVs were removed by washing them three times in PBS. The cytoskeleton and nucleus were stained with DIL and DAPI, respectively. Ultimately, a Zeiss fluorescence microscope was used to produce fluorescent images of the cells.

In vitro Anti-Proliferation Activity of *Pd*-OMVs

To investigate the in vitro antiproliferative activity of *Pd*-OMVs, the CCK-8 assay was performed. CT26, HCT116, and SW480 cells were seeded into 96-well plates and cultured in a cell incubator. After the cells grew to 60%, the original medium was discarded and complete medium containing 0, 100, 200, and 400 μg/mL *Pd*-OMVs was added to the 96-well plates to continue incubation with the cells for 24 and 48 h. Then, 10 μL of WST-8 was added to each well and cocultured with the cells at 37°C for 1 h. Finally, the absorbance of each well was measured at 450 nm.

In vitro Anti- Invasion Activity of *Pd*-OMVs

An 8 mm pore size transwell plate (BIOFIL, Guangzhou) was utilized to conduct the cell invasion assay. Matrigel Basement Membrane Matrix was used to form a coat before seeding the cells. The cells were seeded in serum-free medium and placed in the upper chamber, which was incubated with OMVs at concentrations of 0, 100, 200, and 400 μg/mL, while the lower chamber contained a full medium with 10% FBS. After incubation for 24 h, the cells on the upper surface were removed by swab and the cells on the lower side of transwell were fixed with 4% paraformaldehyde. Invaded cells were stained with crystal violet. Images were taken through an inverted microscope.

Mice

All animal experiments were performed in compliance with the laws and institutional guidelines and approved by the Animal Ethics Committee of Guangzhou University of Chinese Medicine (No. ZYD-2022-075). The male BALB/c mice

(18–22 g) were obtained from Guangdong medical laboratory animal center, China. All mice were kept in specific pathogen-free conditions (temperature of 23 ± 1°C, 12 h light/dark cycle) and allowed free access to water and food. The mice were allowed to acclimate for one week before performing experiments.

To assess the in vivo anti-colon tumor capacity of OMVs, a CT26 colon tumor model was employed. In brief, CT26 cells (1×10^6) were suspended in 100 μL of 1640 medium and subcutaneously inoculated into the right flank of each mouse. Tumor volume and mice body weight were monitored every 2 days. The tumor size was serially measured with a caliper. Tumor volume was calculated as length × width^2 × 0.5.

For CT26 colon tumor inhibition, a total of 24 mice were randomly assigned to four groups with 6 mice per group. When the tumor volume reached about 100 mm^3, mice in the OMVs-10 μg and OMVs-20 μg groups were injected intratumorally with 10 μg or 20 μg protein of OMVs four times every two days, respectively. Mice in the 5-Fu group were injected intraperitoneally with 25 mg/kg of 5-Fu once a day for 7 days. At the end of the experiment, mice were euthanized.

For systemic toxicity evaluation, a total of 24 mice were randomly assigned to four groups with 6 mice per group. When the tumor volume reached approximately 100 mm^3, mice were intravenously injected with OMVs (100 μL) at concentrations of 1.5 or 3 mg protein/kg four times every two days. At the end of the experiment, mice were euthanized.

For the neutralization of CXCL10, a total of 18 mice were randomly divided into PBS, OMVs-20 μg, and OMVs +anti-CXCL10 groups, with 6 mice in each group. Mice in the OMVs+anti-CXCL10 group were injected intraperitoneally with 50 μg of anti-mouse CXCL10 neutralization antibody every 3 days for 2 weeks after inoculation with CT26 cells. When the tumor volume reached about 100 mm^3, mice in the OMVs-20 μg and OMVs+anti-CXCL10 groups were injected intratumorally with 20 μg protein of OMVs four times every two days. At the end of the experiment, mice were euthanized.

Transcriptomics

Mouse tumor tissue was collected for transcriptomics analysis. Detailed methods for transcriptomics analysis can be found in Supplementary Methods. The raw sequencing data have been deposited in the Genome Sequence Archive at BIG Data Center (http://bigd.big.ac.cn/) under the accession number: PRJCA025308.

In vivo Biodistribution of *Pd*-OMVs

For in vivo OMVs distribution, a near-infrared fluorescence probe DIR was used to label these OMVs. CT26 cells (1×10^6) were inoculated subcutaneously into the right flank of mice. When the tumor volume reached about 100 mm^3, mice were administered with DIR-OMVs 3 mg protein/kg per mouse via intravenous injection. At predetermined time points (6, 12, 24 and 48 h), mice were euthanized. The tumors were isolated, and their fluorescence images were taken using an IVIS spectrum imaging system (PerkinElmer/Caliper LifeSciences, Hopkinton, MA, USA).

Quantitative Real-Time PCR (qPCR)

Trizol reagent was used to capture total RNA in accordance with the manufacturer's instructions. Using HiFiScript gDNA Removal RT MasterMix, total RNA was reverse transcribed to cDNA. MagicSYBR Mixture was used for qPCR. Primers used for qPCR were listed in Table S1.

Elisa

ELISA kits were utilized to measure the quantity of IL-6, TNF-α, and IL-1β in the plasma and tumor tissues, following the manufacturer's instructions. These ELISA kits have a sensitivity of less than 20 pg/mL.

H&E and Immunohistochemical (IHC) Staining

For H&E staining, tumor tissues were fixed by 4% paraformaldehyde, embedded in paraffin, and cut into 4-μm-thick sections. The sections were stained with standard hematoxylin and eosin according to the manufacturer's instructions.

For IHC, the tumor slides were blocked with 3% hydrogen peroxide after deparaffinization, rehydration and antigen retrieval. Then, the slides were incubated with the primary (CXCL10, 1:500; CD8, 1:250) and secondary antibodies. The

3.3′-diaminobenzidine and hematoxylin were used for immunohistochemical staining. The sections were photographed by optical microscope and counted with image J software.

Flow Cytometry

Tumor tissues were isolated, resected, longitudinally opened and cut into pieces. The digestion mixture containing 5% FBS, 0.5 mg/mL collagenase type IV, 0.5 mg/mL collagenase type II, 0.25 mg/mL DNase was added to the tumor pieces for 30 min at 37°C. The cell suspensions were centrifuged at 300 × *g* after being filtered through a 70 nm mesh. After that, the cells were stained with antibodies and incubated. Zombie Aqua™ Fixable Viability Kit was used to discriminate live and dead cells. After incubation, cells were washed in PBS buffer and examined with BD LSR Fortessa.

Statistical Analysis

GraphPad Prism 8 was employed for statistical analysis. The experimental data were expressed as mean ± standard error of mean (SEM). For data that conformed to normal distributions, multiple-group comparisons were conducted using one-way ANOVA. Comparisons between groups were carried out by LSD (for data with equal variances) or *Dunnett's T3* (for data with unequal variances). Two-group comparisons were analyzed using a two-tailed *Student's t*-test. Data that did not conform to normal distribution were analyzed using nonparametric tests, and the *Kruskal–Wallis* test was chosen for between-group comparisons. Statistical significance was denoted at *** $p < 0.001$, ** $p < 0.01$, * $p < 0.05$, ns, no significance.

Results

Characterization of Isolated *Pd*-OMVs

Pd-OMVs were isolated and purified from the *Pd* cultures by ultracentrifugation (Figure 1A). TEM images showed that the *Pd*-OMVs exhibited uniform cup-shaped membrane vesicular structures (Figure 1B). The DLS examinations indicated that the average hydrodynamic particle size of *Pd*-OMVs was 165.5 nm. (Figure 1C). Moreover, the zeta potential of *Pd*-OMVs were averaged about –9.56 mV (Figure 1D). Additionally, the protein profiles of both *Pd* and *Pd*-OMVs were identified (Figure 1E). The protein molecular weights of *Pd*-OMV were centrally distributed at 70–100 kDa and above 150 kDa.

Proteins are the important material basis for the pharmacological effects of OMVs.[23] Therefore, we performed a proteomic analysis of the *Pd*-OMVs. The proteomics results showed that a total of 1730 proteins were identified and quantified from the *Pd*-OMVs, and 16,724 peptides were identified (Figure 1F). Furthermore, GO and KEGG databases were utilized for functional annotation of the identified proteins from *Pd*-OMVs. As shown by the results of KEGG annotation analysis in Figure 1G, *Pd*-OMVs contained proteins related to mechanisms such as apoptosis, antigen processing and presentation, and cancer pathways, etc. The results of GO annotation analysis showed that *Pd*-OMVs contained proteins closely related to biological processes such as inflammatory responses, apoptotic processes, and immune system processes (Figure 1H). These results indicate that *Pd*-OMVs were successfully isolated and adequately characterized in this study, and the proteins of *Pd*-OMVs may regulate the signaling pathways of inflammation, immunity, and apoptosis, which provides an important material basis for the pharmacological effects of *Pd*-OMVs.

In vitro Antitumor Activity of *Pd*-OMVs

Effective internalization of OMVs by colon cancer cells is a prerequisite for their antitumor activity. To label *Pd*-OMVs and monitor their biodistribution, a green fluorescence probe DIO was utilized. The images showed that the CT26 cells treated with PBS exhibited no green fluorescence signals. In contrast, cells treated with DIO-OMVs exhibited prominent green signals in the cytoplasm following a 5-hour co-incubation. (Figure 2A). These findings suggested that *Pd*-OMVs can be taken up by CT26 cells.

Subsequently, to assess the impact of *Pd*-OMVs on proliferation of tumor cell lines, the CCK8 assay was utilized. Various concentrations of *Pd*-OMVs were administered to the murine colon cancer cell line CT26. Following co-incubation for 24 and 48 h, *Pd*-OMVs demonstrated a significant concentration-dependent and time-dependent inhibition of CT26 cells proliferation when compared to the OMVs-untreated group. (Figure 2B and C). The proliferative activity of human colon cancer cell lines HCT116 and SW480 was likewise significantly inhibited by *Pd*-OMVs (Figure S1).

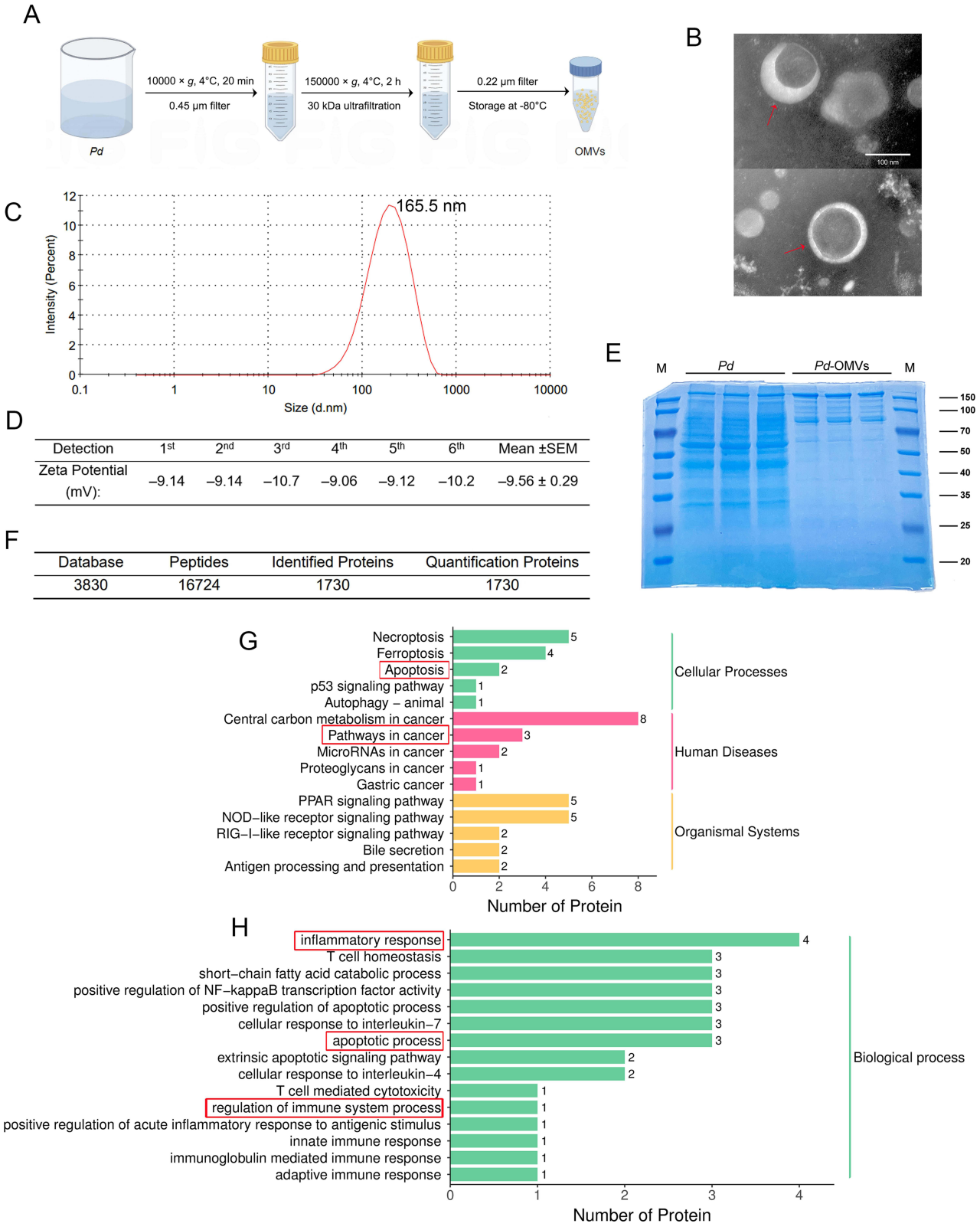

Figure 1 Identification and characterization of *Pd*-OMVs. (**A**) Isolation and purification procedures of *Pd*-OMVs. (**B**) TEM images of *Pd*-OMVs. (**C**) Size distribution of *Pd*-OMVs. (**D**) Zeta potential of *Pd*-OMVs (n = 6). (**E**) Protein profiles of *Pd* and *Pd*-OMVs (n = 3). (**F**) Summary of protein identification results for *Pd*-OMVs. (**G**) KEGG and (**H**) GO enrichment analysis items. The red boxes show the key items related to the proteins of *Pd*-OMVs.

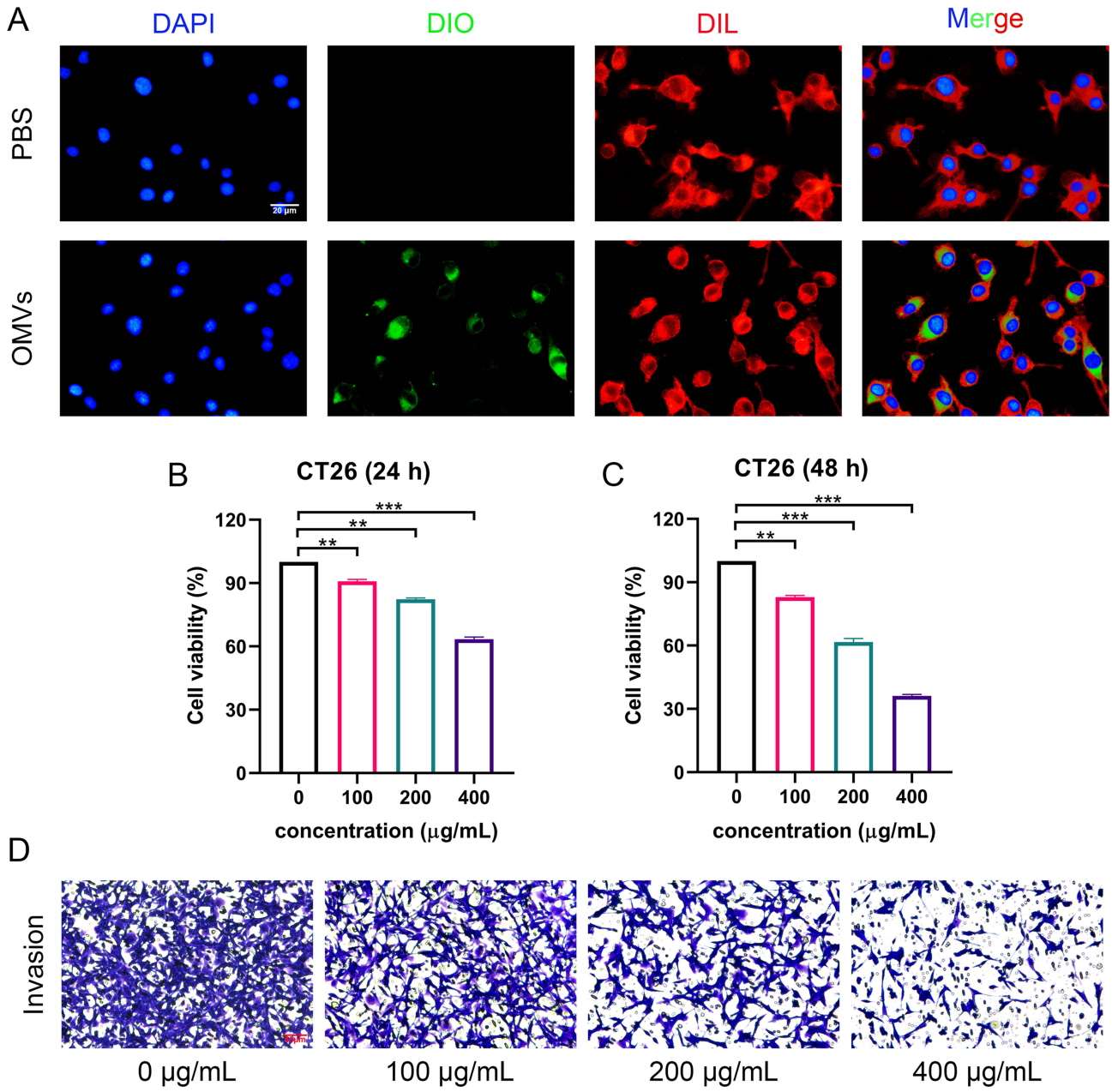

Figure 2 In vitro antitumor activity of *Pd*-OMVs. (**A**) Uptake profiles of *Pd*-OMVs by CT26 cells. Viabilities of CT26 cells after co-incubated with *Pd*-OMVs for (**B**) 24 and (**C**) 48 h. (**D**) Invasion of CT26 cells after co-incubation with *Pd*-OMVs for 24 h. Data are presented as the mean ± SEM (n = 3). $^{**}p < 0.01$, $^{***}p < 0.001$.

Notably, the administration of *Pd*-OMVs resulted in nearly no cytotoxicity in normal colon epithelial cells NCM460, indicating their excellent biocompatibility and specificity to tumor cells. (Figure S2).

To evaluate the impact of *Pd*-OMVs on CT26 cells invasion, transwell assays were conducted. The results revealed that CT26 cells in the OMVs-untreated groups showed extensive invasion, which indicated the intrinsic metastatic activity of the cells. However, *Pd*-OMVs considerably reduced the invasion of CT26 cells in a concentration-dependent manner (Figure 2D). Collectively, these results implied that *Pd*-OMVs have the capability to effectively inhibit the proliferation and invasion of colon tumor.

Inhibitory Effects of *Pd*-OMVs on Colon Tumor

To assess the therapeutic effectiveness and antitumor response of *Pd*-OMVs, we administered specified dosages of OMVs intratumorally four times to mice bearing a CT26 tumor (Figure 3A). As observed in Figure 3B, over the course

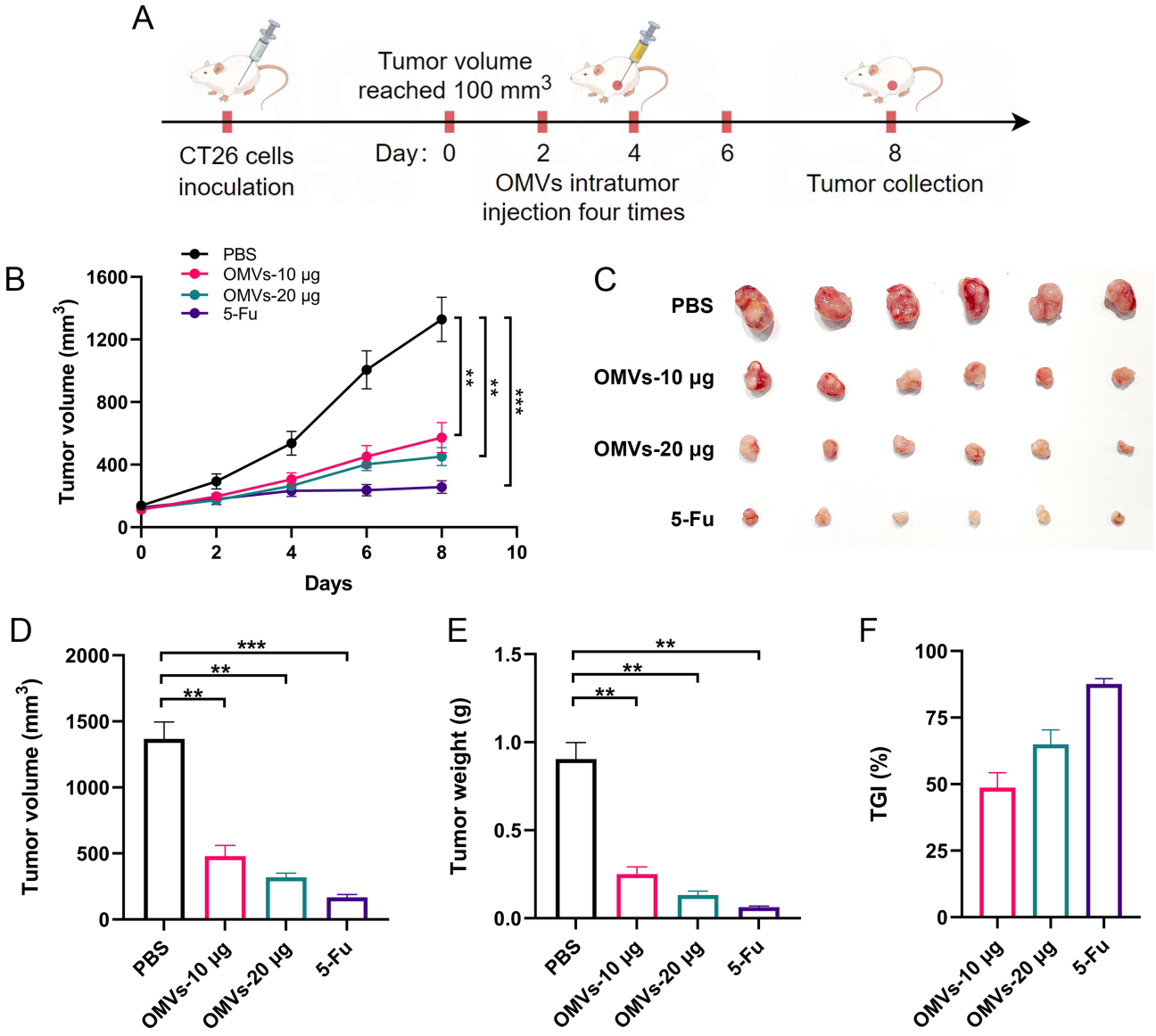

Figure 3 *Pd*-OMVs inhibited colon tumor growth. (**A**) Experimental design for evaluating the anti-colon tumor effects of *Pd*-OMVs given intratumorally. (**B**) Variation of tumor volume within 8 days after intratumoral injection of *Pd*-OMVs. (**C**) Comparison of tumor morphologic features. (**D**) Tumor volume and (**E**) weight on day 8. (**F**) TGI in each treatment group. Data are presented as the mean ± SEM (n = 6). $^{**}p < 0.01$, $^{***}p < 0.001$.

of 8 days, the tumor volume in the PBS group exhibited rapid growth, while the growth trend of tumor was markedly inhibited by *Pd*-OMVs. Furthermore, in a dose-dependent manner, the treatment with *Pd*-OMVs significantly reduced both the tumor volume and weight, consistent with the variation in tumor size observed over the 8-day period. (Figure 3C–E). Compared with the PBS group, 49% and 65% of tumor growth inhibition (TGI) were achieved in the OMVs-10 and 20 μg groups, respectively, whereas 83% of TGI was achieved in the 5-Fu group (Figure 3F). 5-Fu is one of the most commonly used chemotherapeutic agents for colon cancer in recent decades. However, the low bioavailability and severe side effects of 5-Fu significantly affect the patients' quality of life, thus limiting its widespread use in the clinic.[31] In in vivo experiments, mice treated with 5-Fu had significantly lower body weights than mice in the PBS group, reflecting a serious threat to their health, whereas mice treated with *Pd*-OMVs had no significant decrease in body weight (Figure S3). Although the tumor inhibition effect of *Pd*-OMVs was slightly lower than that of 5-Fu, considering the lower toxicity and better biocompatibility of *Pd*-OMVs, the potential of *Pd*-OMVs as a novel antitumor therapy is

obvious. Moreover, in view of the low efficacy rate of existing immunotherapeutic approaches, the development of *Pd*-OMVs as a tumor immunostimulant highlights the importance of practical significance.[6]

Anti-Colon Tumor Mechanisms of *Pd*-OMVs

Transcriptome analysis of tumor tissues was carried out in order to determine the mechanisms how *Pd*-OMVs limit the colon tumor growth. Figure 4A showed that the gene expression profiles of tumor tissues changed significantly after *Pd*-OMVs treatment. As presented in Figure 4B, in comparison to the PBS group, the OMVs-20 μg group exhibited 1318

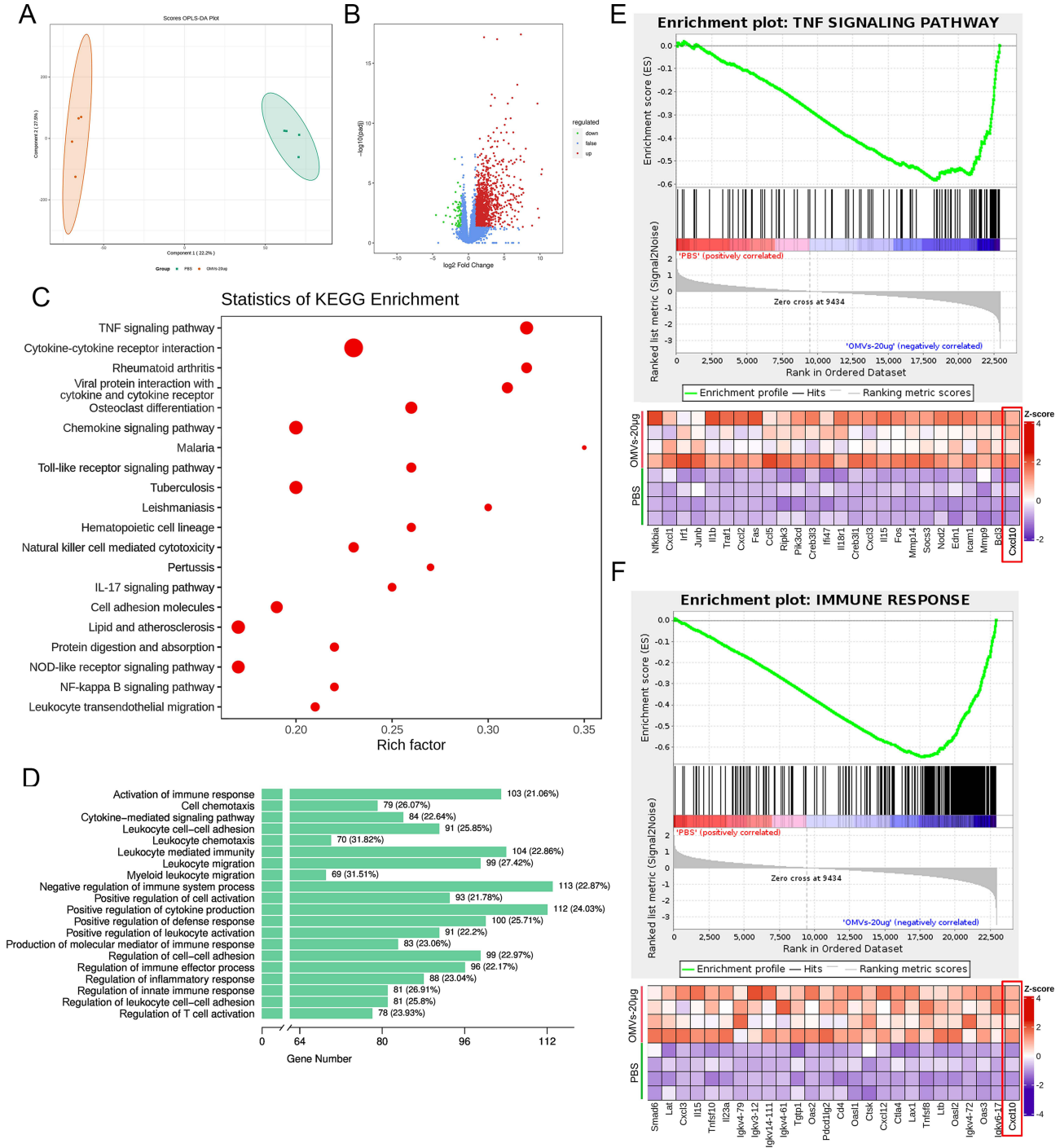

Figure 4 Transcriptome characteristics of tumor tissues treated by *Pd*-OMVs. (**A**) Scores OPLS-DA plot. (**B**) Volcano plot. (**C**) KEGG and (**D**) GO enrichment analysis items. GSEA enrichment plots of (**E**) TNF signaling pathway and (**F**) immune response.

upregulated genes and 64 downregulated genes. To delve deeper into the biological functions of these differentially expressed genes (DEGs), we conducted KEGG and GO analyses by querying the DEGs in each group in the database. Subsequently, we obtained the top 20 enriched terms for both KEGG and GO related to the DEGs. The KEGG analysis revealed that DEGs were highly enriched in the TNF signaling pathway, while the largest number of DEGs were found in the cytokine-cytokine receptor interaction pathway (Figure 4C). In Figure 4D, it was evident that the activation of the immune response pathway in GO enrichment analysis exhibited the most notable difference between the PBS and OMVs-treated groups. These suggested that the antitumor effects of *Pd*-OMVs may rely on the activation of the antitumor immune response.

To delve deeper into the significance of the KEGG and GO enrichment analysis, GSEA analysis was conducted on KEGG and GO datasets. As seen in Figure 4E and F, the TNF signaling pathway and the immune response pathway were enriched in the *Pd*-OMVs-treated group. TNF is a major mediator of apoptosis, inflammation and immunity, regulating multiple signaling pathways including NF-κB, caspases and chemokines.[32] It has been suggested that TNF mediates the antitumor immune response of $CD8^+$ T cells and NK cells, which is consistent with the immune response pathways enriched in the GO database.[33] Notably, these two pathways indicated that CXCL10, a T cell chemoattractant previously described to be involved in modulating the tumor immune environment, was significantly increased in the OMVs-treated group.[34]

The transcriptomics results unveiled a robust enhancement in the antitumor immune response accompanied by a notable upregulation of the chemokine CXCL10 after *Pd*-OMVs administration. To substantiate these findings, we devised corresponding experiments for validation. As depicted in Figure 5A and B, both CXCL10 mRNA and protein expressions in tumor tissues exhibited a substantial increase following OMVs treatment. In accordance with established literature highlighting the pivotal role of CXCL10 as a potent chemokine for $CD8^+$ T cells, known to mediate $CD8^+$ T cells chemotaxis and infiltration.[35,36] We employed flow cytometry to assess the presence of $CD8^+$ T cells in tumor tissues after *Pd*-OMVs administration. Figure 5C and D demonstrated a significant increase in $CD8^+$ and Grb^+CD8^+ T cells in the OMVs-treated group. The results of IHC also confirmed the increase of CXCL10 and $CD8^+$ T cells (Figure 5E and S4). Reports indicated that $CD8^+$ T cells are the most significant antitumor effector cells in the immunotherapy process, exhibiting direct tumor cell killing capabilities and mediating tumor regression.[37,38] Notably, Treg cells and M2-TAMs ($CD206^+$) were markedly reduced after OMVs administration, whereas M1-TAMs ($CD86^+$) were significantly increased (Figure S5). In addition, as presented in Figure 5F and G, the expressions of TNF-α, IL-1β and IL-6 increased remarkably, implying a significant enhancement of antitumor immunity in the OMVs-treated tumor.

CXCL10 Mediated the Anti-Colon Tumor Effects of *Pd*-OMVs

To gain a deeper insight into the function of CXCL10 in the antitumor effects of *Pd*-OMVs, we blocked the biological function of CXCL10 using an anti-CXCL10 neutralization antibody in *Pd*-OMVs-treated mice (Figure 6A). The antitumor effects of *Pd*-OMVs were assessed by comparing the results of the PBS and OMVs-20 μg groups. The critical role of CXCL10 in the antitumor of *Pd*-OMVs was elucidated by comparing the results of OMVs-20 μg and OMVs+anti-CXCL10 groups. As depicted in Figure 6B–D, mice in the PBS group showed faster tumor growth and rapid increase in tumor volume and tumor weight. *Pd*-OMVs treatment significantly inhibited the growth of colon tumors, as evidenced by a significant decrease in tumor volume and tumor weight. However, the inhibitory effect of *Pd*-OMVs on tumor volume and weight was partially attenuated after administration of anti-CXCL10 neutralization antibody. Additionally, the inhibitory effects on tumor growth within 8 days was also partially relieved (Figure 6E). Additionally, ELISA and IHC staining were performed to confirm that the CXCL10 had been largely eliminated in tumor tissues (Figure 6F, G and S6). H&E staining images revealed a significant reduction in CT26 cells in the OMVs-20 μg group, whereas the population of CT26 cells in tumor tissues significantly increased after anti-CXCL10 administration, similar to that in the PBS group (Figure 6G). The increase in CT26 cells showed a negative correlation with the reduced presence of $CD8^+$ T cells in tumor tissues (Figure 6G and S6), indicating that CXCL10 plays a crucial role in controlling the infiltration of $CD8^+$ T cells. Collectively, these results underscore the necessity of CXCL10 for *Pd*-OMVs to exert their inhibitory effects on the growth of colon tumor.

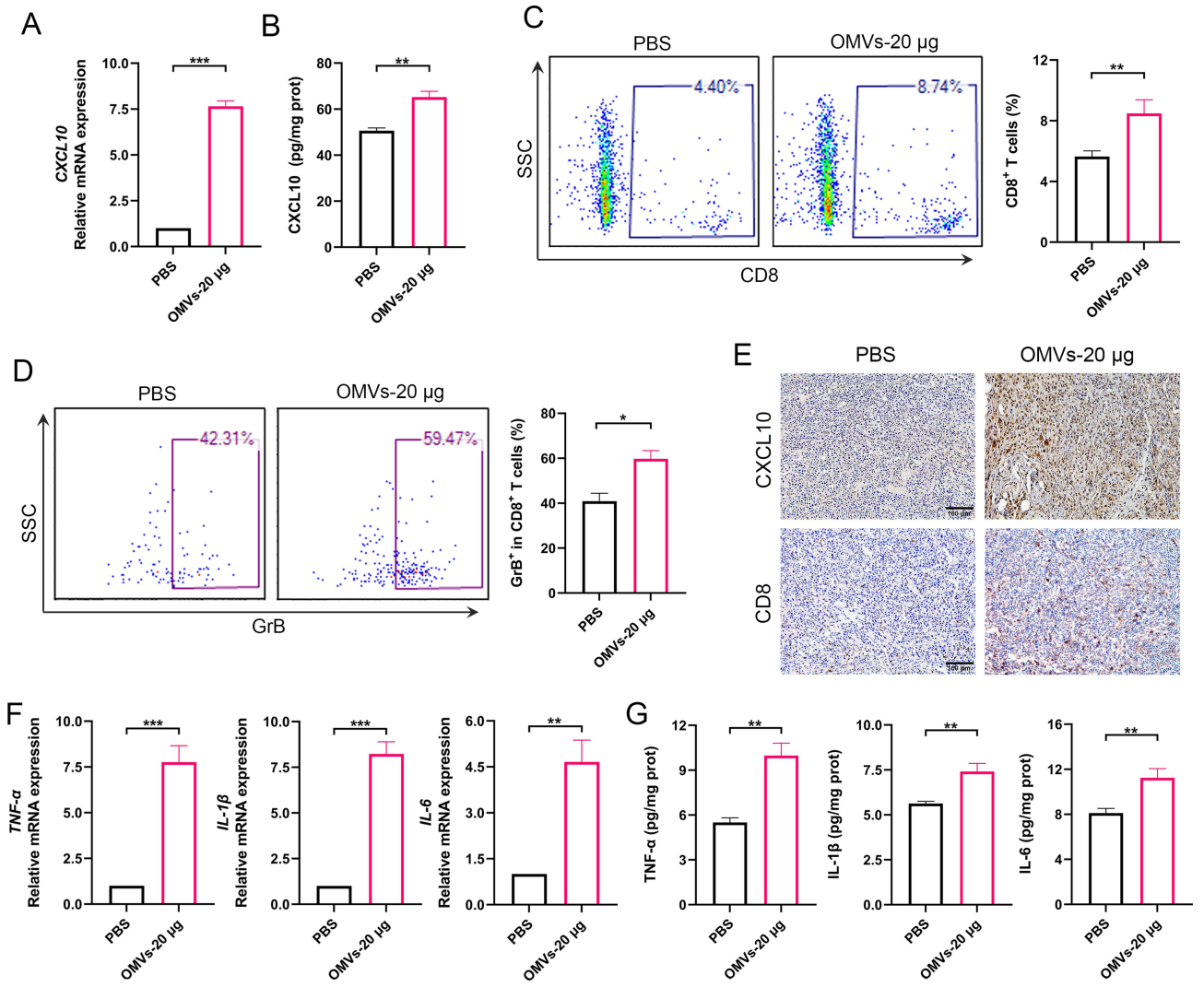

Figure 5 *Pd*-OMVs promoted the expression of CXCL10 subsequently recruiting $CD8^+$ T cells to enhance the antitumor immune response. (**A**) The mRNA expression of *CXCL10*. (**B**) The protein expression of CXCL10. (**C**) $CD8^+$ T cells in tumor tissues. (**D**) GrB^+CD8^+ T cells in tumor tissues. (**E**) IHC images of CXCL10 and CD8. (**F**) The mRNA expressions of *TNF-α*, *IL-1β* and *IL-6*. (**G**) The protein expressions of TNF-α, IL-1β and IL-6. Data are presented as the mean ± SEM (n = 6). $^*p < 0.05$, $^{**}p < 0.01$, $^{***}p < 0.001$.

Anti-Colon Tumor Effects of *Pd*-OMVs Administered Intravenously

In view of their nanoscale size, OMVs may theoretically be able to accumulate passively in the tumor site through the enhanced permeability and retention (EPR) effect. Therefore, it may be feasible to deliver OMVs via intravenous administration. Subsequently, experiments were conducted to observe the tumor accumulation of DIO-labeled OMVs administered via a single intravenous injection. As depicted in Figure 7A, OMVs gradually accumulated in tumor tissues after intravenous injection. The maximum accumulation of OMVs in tumor tissues occurred at 24 h after intravenous administration, and then they were gradually metabolized and cleared.

To further evaluate the therapeutic effects of intravenously administered *Pd*-OMVs on colon tumor, we performed a CT26 colon tumor model (Figure 7B). Tumor volume for the various groups of mice were monitored during the *Pd*-OMVs treatment period. Comparing the *Pd*-OMVs group to the PBS group, there was a noticeable dose-dependent inhibition of tumor growth (Figure 7C–F). Following intravenous injection of *Pd*-OMVs, H&E staining images showed a considerable reduction in the number of CT26 cells, and the nuclei were pyknotic and fragmented, particularly in the OMVs-high group (Figure 7G). Additionally, the in vivo anti-proliferative capability of *Pd*-OMVs was evaluated using Ki67 staining. As depicted in Figure 7G and S7, the number of Ki67 positive cells notably decreased in a dose-dependent manner following *Pd*-OMVs administration.

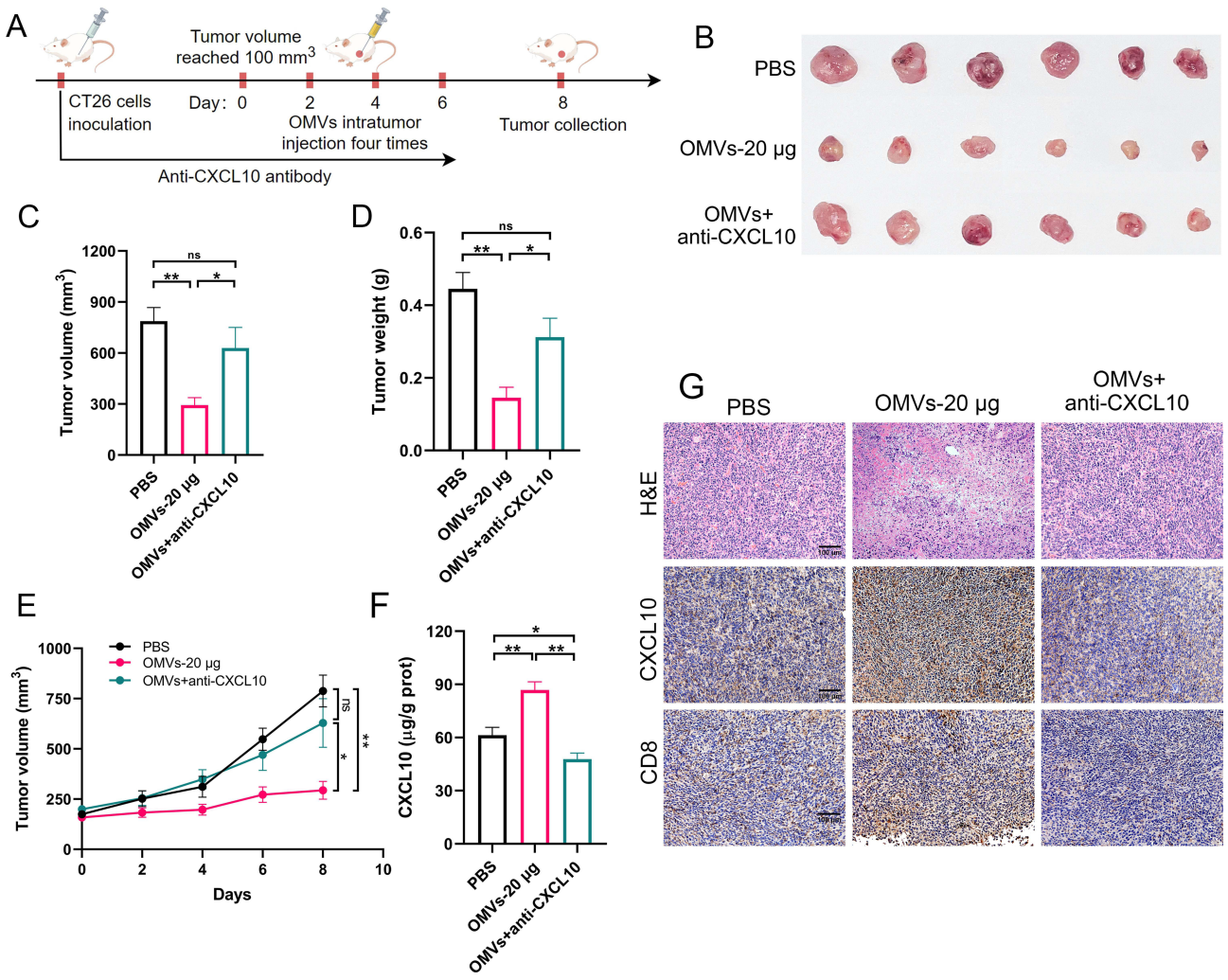

Figure 6 CXCL10 mediated the infiltration of $CD8^+$ T cells and the antitumor effects of *Pd*-OMVs. (**A**) Experimental design for assessing the anti-colon tumor effects of *Pd*-OMVs. Anti-CXCL10 antibody was used to block CXCL10 expression in tumor tissues. (**B**) Comparison of tumor morphologic features. (**C**) Tumor volume and (**D**) weight on day 8 after *Pd*-OMVs administration. (**E**) Variation of tumor volume within 8 days. (**F**) The protein expression of CXCL10 in tumor tissues. (**G**) H&E and IHC images of CXCL10 and CD8. Data are presented as the mean ± SEM (n = 6). $*p < 0.05$, $**p < 0.01$.
Abbreviation: ns, no significance.

Subsequently, the effects of *Pd*-OMVs on CXCL10 expression and $CD8^+$ T cell infiltration after *Pd*-OMVs intravenous injection were verified. As presented in Figure 7H and I, there was a significant increase in the mRNA and protein expressions of CXCL10, resulting in a significant $CD8^+$ T cell infiltration in the tumor tissues. The IHC results also confirmed the increase of CXCL10 and $CD8^+$ T cells (Figure 7G). Meanwhile, the mRNA and protein expressions of TNF-α, IL-1β and IL-6 were dose-dependently upregulated after administration of *Pd*-OMVs, indicating the effective activation of the immune response in tumor tissues (Figure 7J and K). Overall, similar to *Pd*-OMVs administered intratumorally, *Pd*-OMVs given intravenously also exerted significant anti-colon tumor effects by upregulating the expression of CXCL10, which in turn promoted the infiltration of $CD8^+$ T cells in the tumor.

Biosafety Assessment of *Pd*-OMVs

The in vivo safety of *Pd*-OMVs is a fundamental prerequisite for achieving clinical translation. Therefore, we observed alterations in physiological and biochemical parameters in OMVs-treated mice, such as changes in body weight, immune system response, liver and kidney toxicity, and H&E staining in major organs. As illustrated in Figure 8A, the body weight of mice was nearly identical to that of the normal group after *Pd*-OMVs treatment. There was no significant change in plasma pro-inflammatory factors IL-1β and IL-6, while TNF-α exhibited a dose-dependent increase

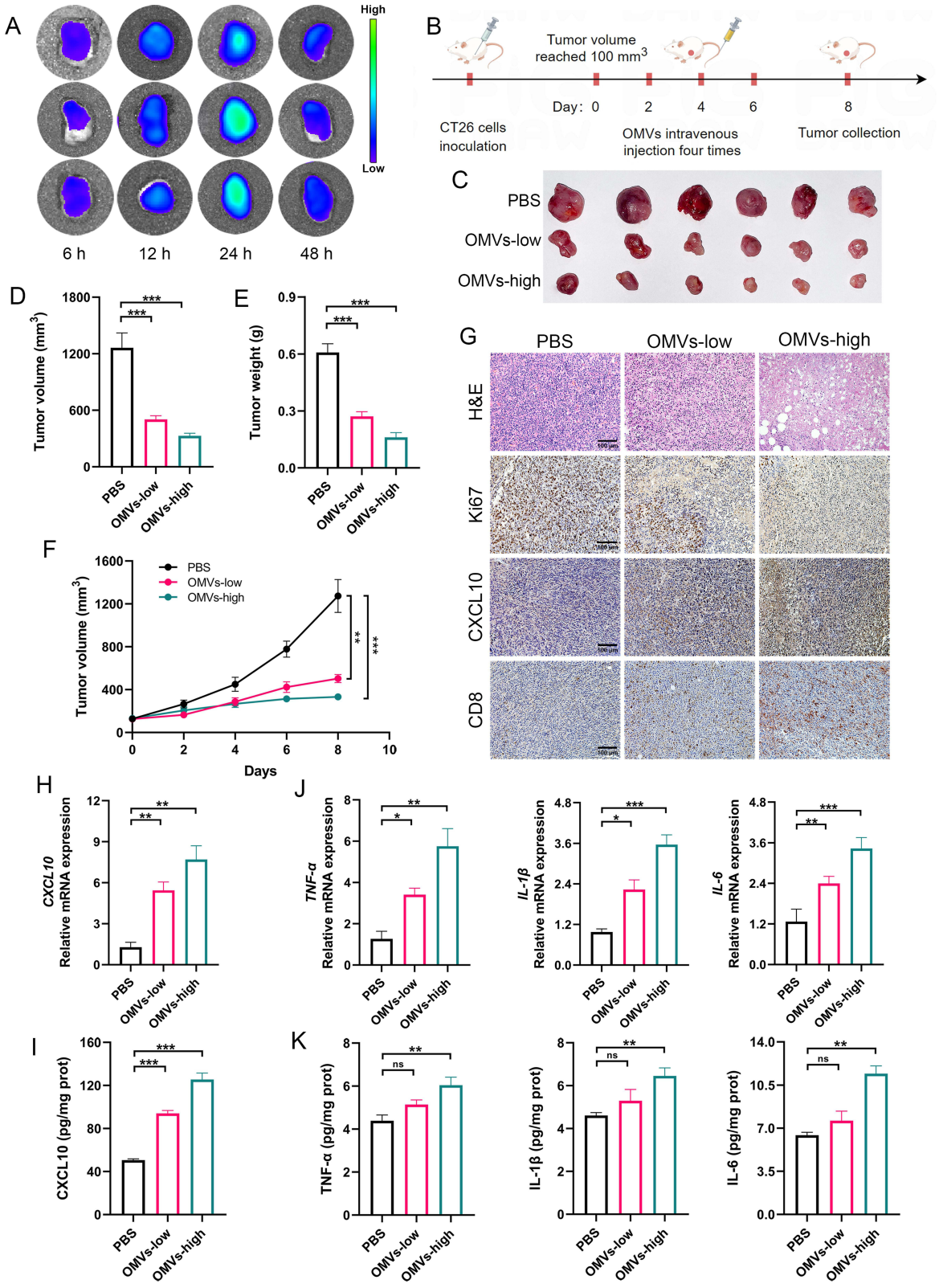

Figure 7 In vivo antitumor effects of *Pd*-OMVs administered intravenously. (**A**) In vivo biodistribution of DIR-loaded *Pd*-OMVs in tumor tissues (n = 3). (**B**) Experimental design for assessing the anti-colon tumor effects of *Pd*-OMVs given intravenously. (**C**) Comparison of tumor morphologic features. (**D**) Tumor volume and (**E**) weight after *Pd*-OMVs intravenous injection. (**F**) Variation of tumor volume within 8 days. (**G**) H&E and IHC images of CXCL10, CD8 and Ki67. The (**H**) mRNA and (**I**) protein expressions of CXCL10. (**J**) The mRNA expressions of *TNF-α, IL-1β* and *IL-6*. (**K**) The protein expressions of TNF-α, IL-1β and IL-6. Data are presented as the mean ± SEM (n = 6). **p* < 0.05, ***p* < 0.01, ****p* < 0.001.

Abbreviation: ns, no significance.

(Figure 8B–D). According to the results of transcriptomics analysis, the TNF signaling pathway is a key pathway for *Pd*-OMVs to exert antitumor effects. And TNF-α, the most core member of the TNF family, carries most of the activities of the TNF family. Therefore, the specific increase of TNF-α in plasma was not only effective in enhancing antitumor immunity, but also necessary for upregulating the expression of the downstream target gene CXCL10.

Furthermore, we examined the kidney and liver toxicity in OMVs-treated mice. BUN and CRE are the main indicators of kidney function. As shown in the Figure 8E and F, there were no significant changes in BUN and CRE after administration of *Pd*-OMVs. ALP, ALT, and AST serve as the main indicators for assessing liver function. As summarized in Figure 8G–I, in comparison to the normal group, the *Pd*-OMVs-treated group exhibited slightly increased concentrations of ALP, ALT, and AST, but the difference between these two groups was not statistically significant. Notably, H&E images of the heart, liver, spleen, lung and kidney of all mouse groups showed no significant tissue damage (Figure 8J).

Discussion

Nowadays, colon cancer stands as one of the most common tumors affecting the digestive tract.[39] Bacteria therapy has emerged as a pivotal element in tumor immunotherapy, playing a substantial role in the prevention and treatment of colon cancer.[40,41] As a second-generation probiotic, *Pd* not only reduces obesity, relieves colitis and type 2 diabetes, but also has significant inhibitory effects on colon cancer.[7] The *Pd*-OMVs, containing biological components of *Pd*, raises the intriguing hypothesis that these vesicles may exhibit the same colon tumor inhibitory effects as *Pd*.

The present study focused on elucidating the anti-colon tumor effects and potential mechanisms of *Pd*-OMVs. *Pd*-OMVs had a cup-shaped structure and an average diameter of about 165.5 nm, which was consistent with the description of OMVs in existing studies, suggesting that the *Pd*-OMVs were successfully extracted by ultracentrifugation.[42] In in vitro experiments, *Pd*-OMVs were taken up by CT26 cells and inhibited the proliferation and invasion of these cells, preliminarily indicating that *Pd*-OMVs have anti-colon tumor activity. Currently, the molecular mechanisms underlying the uptake of OMVs by host cells are not fully understood. It has been shown that host cells internalize OMVs through multiple endocytic pathways, including clathrin-mediated endocytosis, caveola-mediated endocytosis, and clathrin- and caveola-independent endocytosis.[43] Therefore, further studies regarding the potential mechanisms of *Pd*-OMVs uptake by CT26 cells are necessary. Interestingly, the finding that *Pd*-OMVs failed to inhibit the growth of human normal epithelial cells NCM460, suggesting that they may have good tumor cells selectivity by targeting certain pathways in tumor cells. These findings imply that *Pd*-OMVs may exert antitumor effects without affecting the physiological activities of other normal cells, providing good prospects for clinical application.

CXCL10 is a chemokine composed of approximately 50 small (8–14 kDa) secreted proteins.[44] It is a key factor in macrophage and lymphocyte infiltration in cancers and plays an important role in antitumor immunotherapy. CXCL10 acts as a ligand for the CXCR3 receptor, which can be produced by tumor cells and macrophages at the site of tumors and be secreted into the surrounding environment to exert chemotactic effects by binding to its only receptor, CXCR3.[45] CXCR3 is a chemokine receptor that is mainly expressed on the surface of $CD8^+$ T cells.[46] Therefore, $CD8^+$ T cells that highly express CXCR3 can achieve directed migration along a chemical gradient of CXCL10 ligands (known as a chemokine gradient).[47] In this study, *Pd*-OMVs significantly upregulated the expression of CXCL10 in colorectal tumors, leading to the migration of $CD8^+$ T cells and GrB^+CD8^+ T cells to tumor tissues through the chemotactic effect of CXCL10. Thereby, the inhibition of colorectal tumors was achieved through the direct killing of $CD8^+$ T cells and the induction of apoptosis by granzyme B (Figure 9).[48] A related study induced melanoma regression by using a dipeptidyl peptidase 4 inhibitor to increase endogenous levels of CXCL10 indicating the important role of CXCL10 in tumor therapy.[49] Studies have also shown that increased CXCL10 expression at the tumor site is strongly associated with a favorable prognosis in various human cancers, revealing the link between CXCL10 and tumor prognosis.[50] Moreover, considering the potent role of CXCL10 in overcoming drug resistance and enhancing responsiveness to anti-PD-1 therapy, the significant upregulation of CXCL10 by *Pd*-OMVs opens avenues for potential combination therapy with anti-PD-1.[51–53]

$CD8^+$ T cells, as fundamental antitumor effector cells, possess the capability to directly eliminate tumor cells and induce tumor regression.[30] Large-scale $CD8^+$ T cells infiltration into tumor tissues reverses the immune-suppressed status of tumor and induces the transformation of cold tumor into hot ones, which helps to activate tumor immunity.[31]

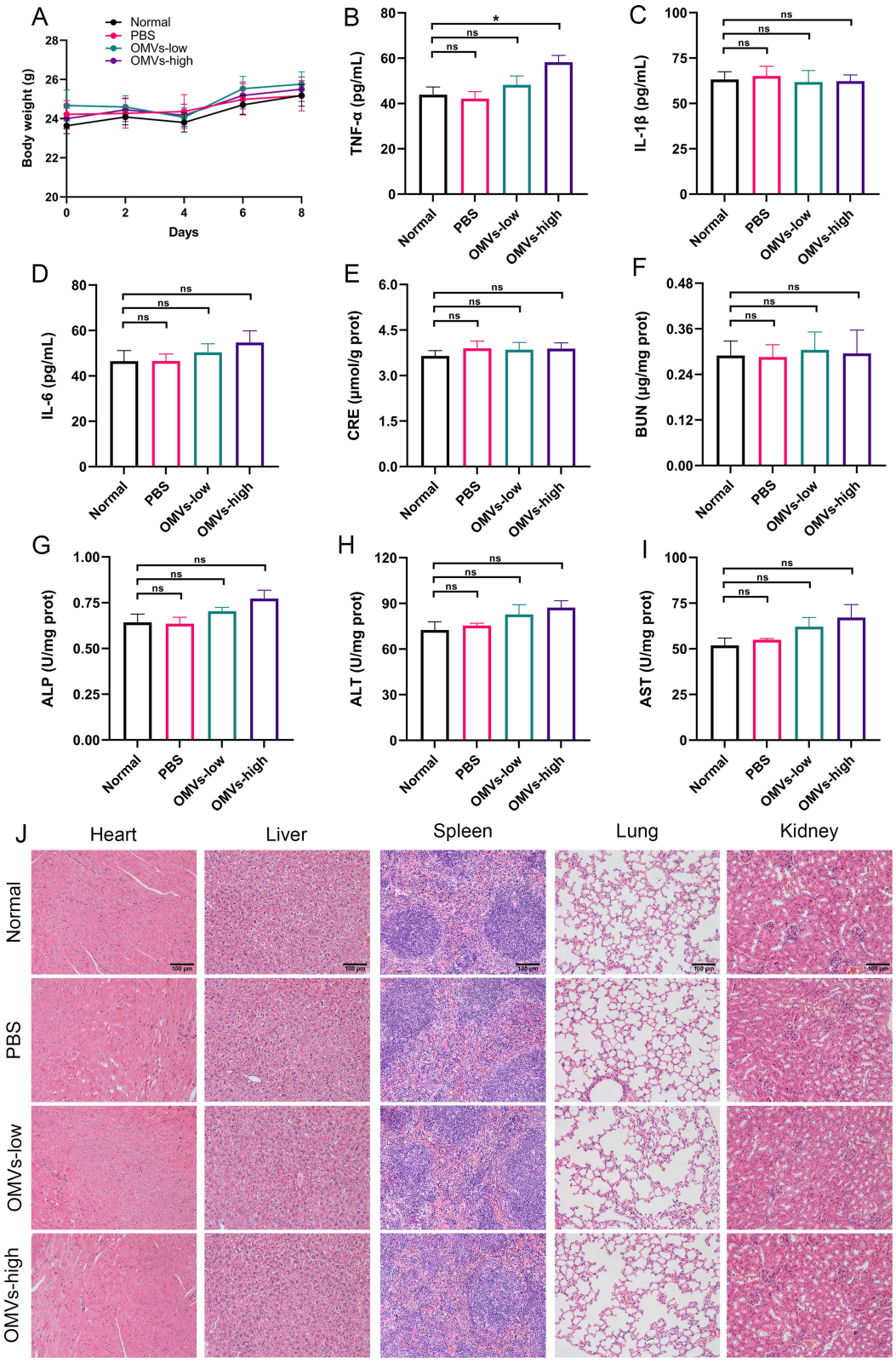

Figure 8 Biosafety evaluation of *Pd*-OMVs in mice. (**A**) Body weight variation in mice after intravenous administration of *Pd*-OMVs. The protein expression of (**B**) TNF-α, (**C**) IL-1β and (**D**) IL-6 in plasma. The levels of (**E**) GRE, (**F**) BUN, (**G**) ALP, (**H**) ALT and (**I**) AST. (**J**) H&E images of heart, liver, spleen, lung and kidney after *Pd*-OMVs administration. Data are presented as the mean ± SEM (n = 6). *$p < 0.05$.

Abbreviation: ns, no significance.

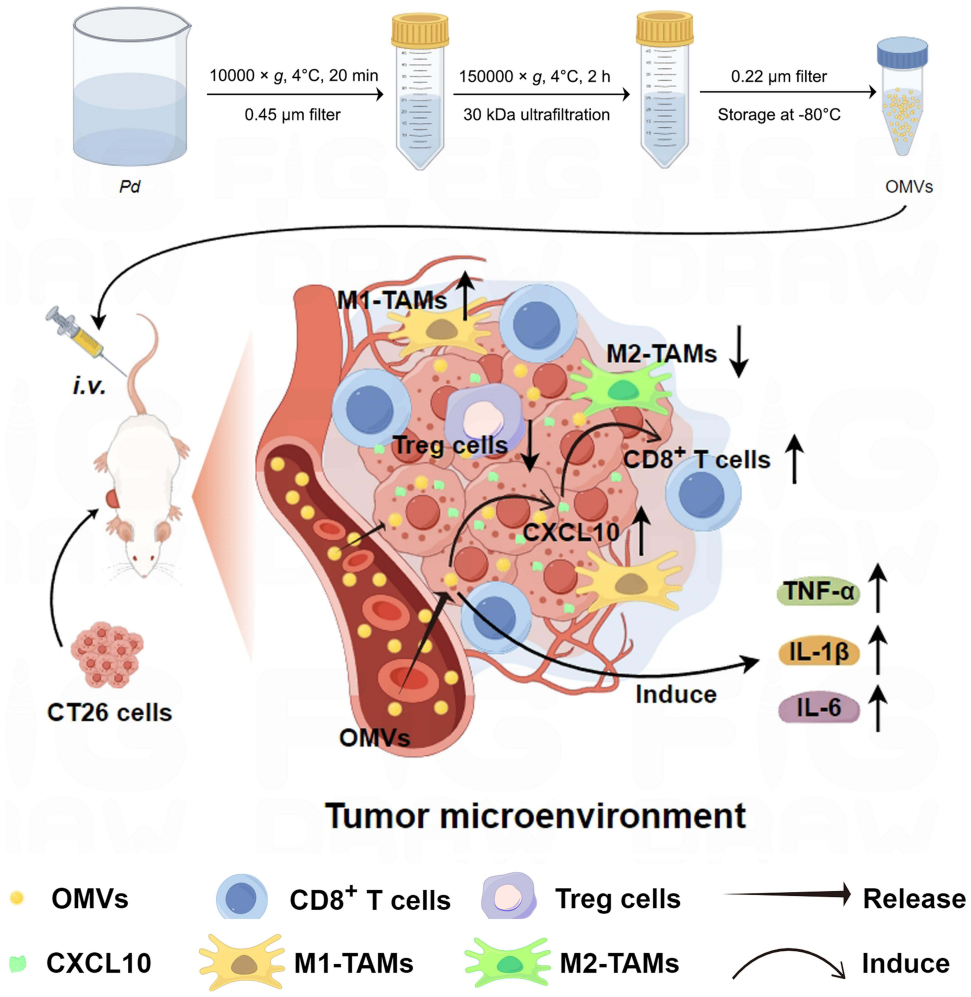

Figure 9 Scheme of the molecular mechanisms underlying *Pd*-OMVs against colon tumor growth (By Figdraw). The *Pd*-OMVs were extracted from *Pd* cultures via ultracentrifugation. After intravenous injection, *Pd*-OMVs reached the tumor site and upregulated the expression of CXCL10, which in turn promoted the migration of $CD8^+$ T cells to tumor tissues and upregulated the expression of pro-inflammatory cytokines. Ultimately, the anti-colon cancer effects of *Pd*-OMVs were achieved by enhancing antitumor immunity.

Bacterial-derived OMVs have been shown to activate the immune response and hold promise for application in antitumor immunotherapy.[54–56] Our findings align with previous research on bacterial-derived OMVs, showcasing their ability to activate the immune response and apply in antitumor immunotherapy.[57] This holds positive implications for clinical translation, further enriching the therapeutic landscape for colon cancer.

To minimize the impact of in vivo metabolism and distribution in mice, we chose to administer OMVs intratumorally for evaluating the efficacy and mechanisms against colon cancer. While intratumoral administration of *Pd*-OMVs addresses concerns related to in vivo metabolism and targeting, providing therapeutic advantages for body surface tumor, its applicability to deep-seated visceral tumors is limited. On the contrary, intravenous administration holds the potential to deliver drugs to both deep-seated tumors and multiple metastatic sites, offering ease of use and convenience for repeated administration. Given the nanoscale size of OMVs, there exists a theoretical possibility that OMVs injected intravenously could leverage the EPR effect for passive accumulation at the tumor site. This speculation led us to investigate whether *Pd*-OMVs could indeed exert effective anti-colon cancer effects through intravenous administration. The results demonstrated that the maximum accumulation of *Pd*-OMVs in tumor occurred 24 h after a single administration. Intriguingly, *Pd*-OMVs administered intravenously exhibited the ability to recruit $CD8^+$ T cells by upregulating CXCL10 expression, consequently enhancing antitumor immunity and ultimately inhibiting tumor growth. These effects mirrored the antitumor efficacy observed with intratumoral administration of *Pd*-OMVs.

The present study innovatively explored the anti-colon cancer effects of *Pd*-OMVs and their underlying mechanism of enhancing antitumor immunity, which provides a solid foundation for the further development of *Pd*-OMVs, but there are still some potential limitations. Here, the inhibitory effect of Pd-OMV on colon cancer has only been investigated using the syngeneic tumor-transplanted mice model. In the future, to comprehensively elucidate the anticancer effect of *Pd*-OMVs on colon cancer, it is necessary to explore the inhibitory effect of *Pd*-OMVs on human colon tumors through patient-derived xenograft models, cell line-derived xenograft models or clinical trials. In addition, more in-depth and comprehensive toxicological studies are required to realize the clinical translation of *Pd*-OMVs.

Furthermore, the development of *Pd*-OMVs as the next generation of cancer immunotherapy agents presents vast possibilities. Previous research has indicated that bacterial-derived OMVs can be easily genetically modified to express a variety of specific molecules on the membrane surface. Additionally, they serve as versatile transport vehicles capable of carrying hydrophilic and hydrophobic cargoes, including chemotherapeutic drugs and siRNAs.[58–60] This versatility enables the loading of hydrophilic payloads into the vesicle core and the encapsulation of endogenous or exogenous hydrophobic antitumor medications (such as paclitaxel) into the phospholipid layer. The potential for combination therapy involving *Pd*-OMVs loaded with chemotherapeutic agents is particularly compelling. Such an approach not only enhances antitumor efficacy but also addresses the issue of chemotherapy-related toxicity. This strategy represents an attractive prospect for future antitumor research, promising improved therapeutic outcomes and reduced side effects.

Conclusion

This study presents a pioneering exploration into the effectiveness and underlying mechanisms of *Pd*-OMVs against colon cancer. To begin with, *Pd*-OMVs were isolated through ultracentrifugation. In vitro investigations demonstrated the internalization of *Pd*-OMVs by CT26 cells, leading to a significant inhibition of cell proliferation and invasion. Subsequent in vivo experiments unveiled that *Pd*-OMVs triggered an upregulation in the expression of CXCL10, facilitating the recruitment of $CD8^+$ T cells to the tumor site. As a result, the antitumor immune response was significantly enhanced, resulting in the inhibition of colon tumor growth. In conclusion, *Pd*-OMVs recruit $CD8^+$ T cells by upregulating the expression of CXCL10, thereby enhancing the antitumor immune response and ultimately inhibiting colon tumor growth. These insights not only expand our understanding of the host benefits derived from probiotic OMVs but also pave the way for innovative avenues in colon cancer treatment. This research significantly contributes to the evolution of probiotic-derived OMVs as a novel immunostimulatory agent in tumor immunotherapy, demonstrating substantial promise for future clinical translation.

Abbreviations

ALP, alkaline phosphatase; ALT, alanine aminotransferase; AST, aspartate aminotransferase; BHI, brain Heart Infusion; BUN, blood urea nitrogen; CRE, creatinine; CXCL10, C-X-C motif chemokine ligand 10; DAPI, 2-(4-Amidinophenyl)-6-indolecarbamidine dihydrochloride; DEGs, differentially expressed genes; DIL, 1.1'-dioctadecyl-3,3,3',3'-tetramethylindocarbocyanine perchlorate; DIO, 3.3′-dioctadecyloxacarbocyanine perchlorate; DLS, dynamic light scattering; EPR, enhanced permeability and retention; 5-Fu, 5-Fluorouracil; GrB, Granzyme B; IHC, immunohistochemical staining; ns, no significance; OMVs, outer membrane vesicles; PBS, phosphate buffered saline; *Pd, Parabacteroides distasonis; Pd*-OMVs, *Pd*-derived OMVs; SEM, standard error of mean; TEM, transmission electron microscopy; TGI, tumor growth inhibition.

Ethics Approval and Informed Consent

The study was supervised and approved by the Animal Ethics Committee of Guangzhou University of Chinese Medicine and conformed to the National Institutes of Health guidelines on the ethical use of animals (Approval No. ZYD-2022-075).

Acknowledgments

This work was supported by the National Natural Science Foundation of China (No. 82174104, 82074142, 22104158), Guangzhou Science and Technology Program (No. 2023B03J1382), Nansha Science and Technology Program (No. 2022ZD004) and Guangdong Basic and Applied Basic Research Foundation (No. 2024A1515011747).

Disclosure

The authors report no conflicts of interest in this work.

References

1. Kim BJ, Hanna MH. Colorectal cancer in young adults. *J Surg Oncol*. 2023;127(8):1247–1251. doi:10.1002/jso.27320
2. Siegel RL, Wagle NS, Cercek A, Smith RA, Jemal A. Colorectal cancer statistics, 2023. *CA Cancer J Clin*. 2023;73(3):233–254. doi:10.3322/caac.21772
3. Puzzono M, Mannucci A, Grannò S, et al. The role of diet and lifestyle in early-onset colorectal cancer: a systematic review. *Cancers*. 2021;13(23):5933. doi:10.3390/cancers13235933
4. Kumar R, Harilal S, Carradori S, Mathew B. A comprehensive overview of colon cancer- a grim reaper of the 21st century. *Curr Med Chem*. 2021;28(14):2657–2696. doi:10.2174/0929867327666201026143757
5. Kim JH. Chemotherapy for colorectal cancer in the elderly. *World J Gastroenterol*. 2015;21(17):5158–5166. doi:10.3748/wjg.v21.i17.5158
6. Kang Y, Li S. Nanomaterials: breaking through the bottleneck of tumor immunotherapy. *Int J Biol Macromol*. 2023;230:123159. doi:10.1016/j.ijbiomac.2023.123159
7. WU WK. Parabacteroides distasonis: an emerging probiotic? *Gut*. 2023;72(9):1635–1636. doi:10.1136/gutjnl-2022-329386
8. Ezeji JC, Sarikonda DK, Hopperton A, et al. Parabacteroides distasonis: intriguing aerotolerant gut anaerobe with emerging antimicrobial resistance and pathogenic and probiotic roles in human health. *Gut Microbes*. 2021;13(1):1922241. doi:10.1080/19490976.2021.1922241
9. Wang K, Liao M, Zhou N, et al. Parabacteroides distasonis alleviates obesity and metabolic dysfunctions via production of succinate and secondary bile acids. *Cell Rep*. 2019;26(1):222–235. doi:10.1016/j.celrep.2018.12.028
10. Cuffaro B, Assohoun ALW, Boutillier D, et al. In vitro characterization of gut microbiota-derived commensal strains: selection of Parabacteroides distasonis strains alleviating TNBS-induced colitis in mice. *Cells*. 2020;9(9):2104. doi:10.3390/cells9092104
11. Liu D, Zhang S, Li S, et al. Indoleacrylic acid produced by Parabacteroides distasonis alleviates type 2 diabetes via activation of AhR to repair intestinal barrier. *BMC Biol*. 2023;21(1):90. doi:10.1186/s12915-023-01578-2
12. Sun H, Guo Y, Wang H, et al. Gut commensal Parabacteroides distasonis alleviates inflammatory arthritis. *Gut*. 2023;72(9):1664–1677. doi:10.1136/gutjnl-2022-327756
13. Zhao Q, Dai MY, Huang RY, et al. Parabacteroides distasonis ameliorates hepatic fibrosis potentially via modulating intestinal bile acid metabolism and hepatocyte pyroptosis in male mice. *Nat Commun*. 2023;14(1):1829. doi:10.1038/s41467-023-37459-z
14. Koh GY, Kane A, Lee K, et al. Parabacteroides distasonis attenuates toll-like receptor 4 signaling and Akt activation and blocks colon tumor formation in high-fat diet-fed azoxymethane-treated mice. *Int, J, Cancer*. 2018;143(7):1797–1805. doi:10.1002/ijc.31559
15. Koh GY, Kane AV, Wu X, Crott JW. Parabacteroides distasonis attenuates tumorigenesis, modulates inflammatory markers and promotes intestinal barrier integrity in azoxymethane-treated A/J mice. *Carcinogenesis*. 2020;41(7):909–917. doi:10.1093/carcin/bgaa018
16. Huang X, Pan J, Xu F, et al. Bacteria-based cancer immunotherapy. *Adv Sci*. 2021;8(7):2003572. doi:10.1002/advs.202003572
17. Weng Z, Yang N, Shi S, et al. Outer membrane vesicles from Acinetobacter baumannii: biogenesis, functions, and vaccine application. *Vaccines*. 2023;12(1):49. doi:10.3390/vaccines12010049
18. Li M, Zhou H, Yang C, et al. Bacterial outer membrane vesicles as a platform for biomedical applications: an update. *J Control Release*. 2020;323:253–268. doi:10.1016/j.jconrel.2020.04.031
19. Li P, Peng T, Xiang T, et al. Klebsiella pneumoniae outer membrane vesicles induce strong IL-8 expression via NF-κB activation in normal pulmonary bronchial cells. *Int Immunopharmacol*. 2023;121:110352. doi:10.1016/j.intimp.2023.110352
20. Liu G, Ma N, Cheng K, et al. Bacteria-derived nanovesicles enhance tumour vaccination by trained immunity. *Nat Nanotechnol*. 2023;19(3):387–398. doi:10.1038/s41565-023-01553-6
21. Holst J, Oster P, Arnold R, et al. Vaccines against meningococcal serogroup B disease containing outer membrane vesicles (OMV): lessons from past programs and implications for the future. *Hum Vaccin Immunother*. 2013;9(6):1241–1253. doi:10.4161/hv.24129
22. Won S, Lee C, Bae S, et al. Mass-produced gram-negative bacterial outer membrane vesicles activate cancer antigen-specific stem-like $CD8^+$ T cells which enables an effective combination immunotherapy with anti-PD-1. *J Extracell Vesicles*. 2023;12(8):e12357. doi:10.1002/jev2.12357
23. Kim OY, Park HT, Dinh NTH, et al. Bacterial outer membrane vesicles suppress tumor by interferon-γ-mediated antitumor response. *Nat Commun*. 2017;8(1):626. doi:10.1038/s41467-017-00729-8
24. Alaniz RC, Deatherage BL, Lara JC, Cookson BT. Membrane vesicles are immunogenic facsimiles of Salmonella typhimurium that potently activate dendritic cells, prime B and T cell responses, and stimulate protective immunity in vivo. *J Immunol*. 2007;179(11):7692–7701. doi:10.4049/jimmunol.179.11.7692
25. Tong Q, Li K, Huang F, et al. Extracellular vesicles hybrid plasmid-loaded lipid nanovesicles for synergistic cancer immunotherapy. *Mater Today Bio*. 2023;23:100845. doi:10.1016/j.mtbio.2023.100845
26. Mehta JP, Ayakar S, Singhal RS. The potential of paraprobiotics and postbiotics to modulate the immune system: a review. *Microbiol Res*. 2023;275:127449. doi:10.1016/j.micres.2023.127449
27. Chen Y, Xu Y, Zhong H, et al. Extracellular vesicles in Inter-Kingdom communication in gastrointestinal cancer. *Am J Cancer Res*. 2021;11(4):1087–1103.
28. Liu Y, Defourny KAY, Smid EJ, Abee T. Gram-positive bacterial extracellular vesicles and their impact on health and disease. *Front Microbiol*. 2018;9:1502. doi:10.3389/fmicb.2018.01502

29. Juodeikis R, Carding SR. Outer membrane vesicles: biogenesis, functions, and issues. *Microbiol Mol Biol Rev*. 2022;86(4):e0003222. doi:10.1128/mmbr.00032-22
30. Wang Y, Deng J, Wang X, et al. Isolation, identification, and proteomic analysis of outer membrane vesicles of Riemerella anatipestifer SX-1. *Poult Sci*. 2024;103(6):103639. doi:10.1016/j.psj.2024.103639
31. Valencia-Lazcano AA, Hassan D, Pourmadadi M, et al. 5-Fluorouracil nano-delivery systems as a cutting-edge for cancer therapy. *Eur J Med Chem*. 2023;246:114995. doi:10.1016/j.ejmech.2022.114995
32. Chen G, Goeddel DV. TNF-R1 signaling: a beautiful pathway. *Science*. 2002;296(5573):1634–1635. doi:10.1126/science.1071924
33. Kearney CJ, Vervoort SJ, Hogg SJ, et al. Tumor immune evasion arises through loss of TNF sensitivity. *Sci Immunol*. 2018;3(23):eaar3451. doi:10.1126/sciimmunol.aar3451
34. Nagarsheth N, Wicha MS, Zou W. Chemokines in the cancer microenvironment and their relevance in cancer immunotherapy. *Nat Rev Immunol*. 2017;17(9):559–572. doi:10.1038/nri.2017.49
35. Loetscher M, Gerber B, Loetscher P, et al. Chemokine receptor specific for IP10 and mig: structure, function, and expression in activated T-lymphocytes. *J Exp Med*. 1996;184(3):963–969. doi:10.1084/jem.184.3.963
36. Weng Y, Siciliano SJ, Waldburger KE, et al. Binding and functional properties of recombinant and endogenous CXCR3 chemokine receptors. *J Biol Chem*. 1998;273(29):18288–18291. doi:10.1074/jbc.273.29.18288
37. Philip M, Schietinger A. $CD8^+$ T cell differentiation and dysfunction in cancer. *Nat Rev Immunol*. 2022;22(4):209–223. doi:10.1038/s41577-021-00574-3
38. Wang Q, Qin Y, Li B. $CD8^+$ T cell exhaustion and cancer immunotherapy. *Cancer Lett*. 2023;559:216043. doi:10.1016/j.canlet.2022.216043
39. Sung H, Ferlay J, Siegel RL, et al. Global cancer statistics 2020: GLOBOCAN estimates of incidence and mortality worldwide for 36 cancers in 185 countries. *CA Cancer J Clin*. 2021;71(3):209–249. doi:10.3322/caac.21660
40. Li W, Deng X, Chen T. Exploring the modulatory effects of gut microbiota in anti-cancer therapy. *Front Oncol*. 2021;11:644454. doi:10.3389/fonc.2021.644454
41. Zhao M, Chen X, Yang Z, Yang X, Peng Q. Bacteria and tumor: understanding the roles of bacteria in tumor genesis and immunology. *Microbiol Res*. 2022;261:127082. doi:10.1016/j.micres.2022.127082
42. Théry C, Amigorena S, Raposo G, Clayton A. Isolation and characterization of exosomes from cell culture supernatants and biological fluids. *Curr Protoc Cell Biol*. 2006;3:22.
43. Sartorio MG, Pardue EJ, Feldman MF, Haurat MF. Bacterial outer membrane vesicles: from discovery to applications. *Annu Rev Microbiol*. 2021;75(1):609–630. doi:10.1146/annurev-micro-052821-031444
44. Zumwalt TJ, Arnold M, Goel A, Boland CR. Active secretion of CXCL10 and CCL5 from colorectal cancer microenvironments associates with GranzymeB+ $CD8^+$ T-cell infiltration. *Oncotarget*. 2015;6(5):2981–2991. doi:10.18632/oncotarget.3205
45. House IG, Savas P, Lai J, et al. Macrophage-derived CXCL9 and CXCL10 are required for antitumor immune responses following immune checkpoint blockade. *Clin Cancer Res*. 2020;26(2):487–504. doi:10.1158/1078-0432.CCR-19-1868
46. Karin N. CXCR3 ligands in cancer and autoimmunity, chemoattraction of effector T cells, and beyond. *Front Immunol*. 2020;11:976. doi:10.3389/fimmu.2020.00976
47. Balkwill F. Cancer and the chemokine network. *Nat Rev Cancer*. 2004;4(7):540–550. doi:10.1038/nrc1388
48. Li Z, Ma R, Tang H, et al. Therapeutic application of human type 2 innate lymphoid cells via induction of granzyme B-mediated tumor cell death. *Cell*. 2024;187(3):624–641.e623. doi:10.1016/j.cell.2023.12.015
49. Barreira da Silva R, Laird ME, Yatim N, Fiette L, Ingersoll MA, Albert ML. Dipeptidylpeptidase 4 inhibition enhances lymphocyte trafficking, improving both naturally occurring tumor immunity and immunotherapy. *Nat Immunol*. 2015;16(8):850–858. doi:10.1038/ni.3201
50. Bronger H, Singer J, Windmüller C, et al. CXCL9 and CXCL10 predict survival and are regulated by cyclooxygenase inhibition in advanced serous ovarian cancer. *Br J Cancer*. 2016;115(5):553–563. doi:10.1038/bjc.2016.172
51. Li X, Lu M, Yuan M, et al. CXCL10-armed oncolytic adenovirus promotes tumor-infiltrating T-cell chemotaxis to enhance anti-PD-1 therapy. *Oncoimmunology*. 2022;11(1):2118210. doi:10.1080/2162402X.2022.2118210
52. Xu X, Zhang Z, Du J, et al. Recruiting T-cells toward the brain for enhanced glioblastoma immunotherapeutic efficacy by co-delivery of cytokines and immune checkpoint antibodies with macrophage-membrane-camouflaged nanovesicles. *Adv Mater*. 2023;35(25):e2209785.
53. Lu S, Xu J, Zhao Z, et al. Dietary Lactobacillus rhamnosus GG extracellular vesicles enhance antiprogrammed cell death 1 (anti-PD-1) immunotherapy efficacy against colorectal cancer. *Food Funct*. 2023;14(23):10314–10328. doi:10.1039/D3FO02018E
54. Xu W, Hao X, Li Y, et al. Safe induction of acute inflammation with enhanced antitumor immunity by hydrogel-mediated outer membrane vesicle delivery. *Small Methods*;2024. e2301620. doi:10.1002/smtd.202301620
55. Su LY, Tian Y, Zheng Q, et al. Anti-tumor immunotherapy using engineered bacterial outer membrane vesicles fused to lysosome-targeting chimeras mediated by transferrin receptor. *Cell Chem Biol*. 2024;24:00038.
56. Chen X, Li P, Luo B, et al. Surface mineralization of engineered bacterial outer membrane vesicles to enhance tumor photothermal/immunotherapy. *ACS Nano*. 2024;18(2):1357–1370. doi:10.1021/acsnano.3c05714
57. Qing S, Lyu C, Zhu L, et al. Biomineralized bacterial outer membrane vesicles potentiate safe and efficient tumor microenvironment reprogramming for anticancer therapy. *Adv Mater*. 2020;32(47):e2002085.
58. Pan J, Li X, Shao B, et al. Self-blockade of PD-L1 with bacteria-derived outer-membrane vesicle for enhanced cancer immunotherapy. *Adv Mater*. 2022;34(7):e2106307. doi:10.1002/adma.202106307
59. Jiang S, Fu W, Wang S, Zhu G, Wang J, Ma Y. Bacterial outer membrane vesicles loaded with Perhexiline suppress tumor development by regulating tumor-associated macrophages repolarization in a synergistic way. *Int J Mol Sci*. 2023;24(13):11222. doi:10.3390/ijms241311222
60. Kuerban K, Gao X, Zhang H, et al. Doxorubicin-loaded bacterial outer-membrane vesicles exert enhanced anti-tumor efficacy in non-small-cell lung cancer. *Acta Pharm Sin B*. 2020;10(8):1534–1548. doi:10.1016/j.apsb.2020.02.002